CHINESE JOURNAL OF PHYSICS VOL. 28, NO. 1 FEBRUARY 1990

Structure and Superconducting Properties in NbN this Films and Single Crystal Oxide Superconductors

Jenh-Yih Juang (莊振益)
Department of Electrophysics, National Chiao-Tung University
Hsinchu, Taiwan 30050, R. 0. C.
(Received Jan. 20, 1990)

While the stable, high performance superconducting properties displayed by sputtered NbN thin fiis have made it a material of technological interest, the critical field anisotropy commonly observed in this material has been a puzzling effect for some time. Systematic studies of the detailed angular dependence of the upper critical field on films with distinct microstructures have disclosed the origin of the observed critical field anisotropy. Detailed analysis within the framework of the Ginzburg-Landau phenomenological theory will be presented. In contrast to the sputtered NbN thin films, the anisotropic nature displayed by the newly discovered high-T_c oxide superconductors is far more pronounced and is believed to be intrinsic to the layered crystal structure. Experimental results on the effects of the critical field anisotropy in M-substituted YBCO single crystals as well as the unusual field orientation dependent current-voltage characteristics in BSCCO (2212) single crystals will be presented.

I. INTRODUCTION

The high performance superconductor NbN is currently being developed for use in both high field magnet[1,2] and superconducting microelectronics applications.[3-5] For magnet applications NbN has the high critical field (H_{c2}) and critical current values necessary for conductor design, and has been shown to be much less susceptible to degradation from either strain[6] or radiation[7,8] than Al 5 materials with similar properties. These have become important factors especially for the application of the magnetic-field-confined plasma fusion reactor. For use in microelectronics applications such as the electrodes in Josephson junctions, NbN can be made with an acceptably high critical temperature (T,) even when deposited at a comparatively low substrate temperature ($\approx 300°C$).[9] For either application the ease of formation makes NbN a highly attractive alternative to other materials such as the Al 5 superconductors and even the newly discovered high-T, superconductors.

In most instances, NbN is deposited as thin film by the reactive sputtering of Nb in a partial pressure of nitrogen. While the specific deposition conditions needed to produce high T_c material will be system dependent. the parameters having the strongest effects on

the T_c of the material are the substrate temperature. the partial pressure of nitrogen, and the deposition rate. Surprisingly, as will be discussed below. the morphology of NbN thin films obtained from different deposition conditions also plays an important role in the transport and superconducting properties of this material. For instance, the upper critical field is commonly found to be anisotropic in polycrystalline films despite the well known cubic (B1; NaCℓ) crystal structure of this material and the macroscopic nature of superconductivity. In the first part of this report we will demonstrate exclusively how the film microstructure affects the H_{c2} of this material *via* the detailed analysis of the angular dependence of H_{c2} using a simple model derived from the Ginzburg-Landau (GL) phenomenological theory .

In contrast to that in NbN thin films, the anisotropic behavior in both the transport and superconducting properties in the high-T, oxides are believed to be originated from the intrinsic layered crystal structure. As a result, many profound effects on the fundamental physical properties of these oxides are expected. Indeed, effects such as the thermodynamic fluctuation in conductivity," the giant flux-creep" and the quasi-two-dimensional behavior induced Kosterlitz-Thouless transition of vortex structure[12,13] and flux-line-lattice melting[14] have been reported based on the layered structure and short coherence length of the oxide family. In addition, as will be demonstrated in this report, despite the poor knowledge of the underlying superconducting mechanisms in these new superconductors, many of the experimental results can still be understood within the scope of the GL theory.

In the second part of this report we present some H_{c2} results of the undoped and Aℓ-doped single crystal YBCO. It is found that the anisotropy ratio as well as the detailed angular dependence on the H_{c2} can be reconciled very well by the anisotropic GL equations developed in the previous part and shows a three-dimensional behavior for both doped and undoped YBCO crystals in the temperature range studied. The effect of Aℓ-substitution, however, is quite dramatic in the H_{c2} of this material and its physical implications as deduced from the Ginzburg-Landau-Abrikosov-Gor'kov (GLAG) theory will be discussed. As a comparative example for the effects of the crystal structure in determining the superconducting properties similar results conducted in single crystal BSCCO (22 12) will also be presented. We found that, due to its more two-dimensional-like crystal structure and possibly shorter coherence length, the experimental determination of the H_{c2} is largely complicated by the more severe flux flow and/or flux creep effects. The dramatic change in current-voltage characteristics as a function of the orientation of the applied magnetic field suggests that intensive studies concerning flux pinning are mostly needed in order to have any practical applications using these materials.

II. NbN THIN FILMS

11-l Experiments And Sample Preparation

The NbN thin films used in this study were provided by three different sources: AT&T Bell Laboratories (Dr. R. B. van Dover), Westinghouse R&D Center (Dr. J. Talvacchio). and

Argonne National Laboratories (Dr. D. W. Capone II[2]). Detailed deposition conditions and the resulting film microstructures can be found elsewhere.[15-17] Briefly, depending on the deposition conditions and the substrate temperatures chosen, three different types of film microstructure were obtained: fine dense equiaxed randomly oriented grains structure, textured (usually in the <111> orientation) columnar grains with typically few nanometer wide columnar intergranular regions, and epitaxially grown single crystal films. Besides the structural characterizations both the normal state transport and the superconducting properties of these films were also examined. Details of the physical properties for the films used can be found in our earlier publication.[18] It was found except for the single crystal films most NbN films display an exceedingly high in-plane resistivity; ranges from 200 $\mu\Omega$-cm to 2000 $\mu\Omega$-cm for samples with similar T_c. This range of resistivity greatly exceeds the maximum value of that calculated for NbN by Hake[19] using a semi-classical model: ρ_{max} = 250 $\mu\Omega$-cm. The "excess" resistivity is usually attributed to the grain boundary resistivity, as indicative in the residual resistivity ratio showing an activated conduction behavior. As will be seen in the following it is this "external" component that gives rise to the H_{c2} anisotropy in sputtered NbN thin films.

The critical field measurements were performed with a standard four-probe technique by passing a minimum constant dc current through the sample, and detecting the resistive transition upon the application of an external field.' Unless specified otherwise the definition used. to determine the H_{c2} is the midpoint of the resistive, transition. The sample temperature was measured in zero field using a carbon-glass resistance thermometer and was controlled in field with a capacitance thermometer. In measuring the angular dependence of the H_{c2}, the cryostat was placed on a rotating table to vary the direction of the applied field relative to the film surface. The angular resolution with this set-up is better than half a degree. The measurements were performed mostly at the Francis Bitter National Magnet Laboratory operated by Massachusetts Institute of Technology.

II-2 Results and Discussion

As has been mentioned, the anisotropy in H_{c2} for NbN has been known for some time but there have been only few attempt to learn its origin. Physically, one would expect that any fundamental anisotropy in the H_{c2}, if existing at all, should vanish (be averaged out) in a very dirty or polycrystalline material such as the NbN films being considered here. Thus this unexpected behavior has been attributed to the columnar grain structure usually obtained in sputtered NbN films, as originally proposed by Ashkin and co-workers.[20] In their model the geometric pair-breaking effects arisen from the presence of isolated columnar grains with at least one of the grain dimensions being comparable to the Ginzburg-Landau coherence length ($\xi_{GL}(T)$). For NbN, $\xi_{GL}(0)$ is estimated to be $\approx$5 nm. The physical validity of this model, however, suffers severe inconsistencies; since the grain size of the columns ($\approx$ 8nm) was much larger than ξ_{GL}, besides the specific grain structure required. It seemed that the easiest way to test this is to investigate the same physical properties using films with distinctly different grain structures. As an example, Fig. 1 shows the result of the $H_{c2}(T)$ with field being applied both parallel and perpendicular to the film surface, for a

non-columnar film. While the general feature of the temperature dependence and the anisotropic character (H_{c2} (T,⊥) > H_{c2}(T,∥)) of the H_{c2} are similar to that observed in Ref. 20, the distinct film microstructure suggests that other mechanisms must be considered.

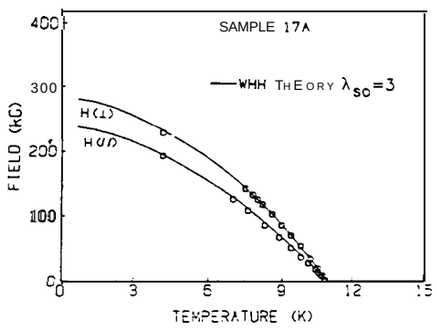

FIG. 1. The temperature dependence of the upper critical field for sample 17A. Data for this non-columnar sample reproduces both the anisotropic and the possible Pauli limiting characteristics in H_{c2}(T) as those observed in films with columnar-void microstructures (see e.g., Ref.20).

Within the framework of the linearized GL equation, relations have been developed to account for the detailed angular dependence of the upper critical field($H_{c2}(\theta)$) resulting from different effects that give rise to the critical field anisotropy. Most of these were worked out in the 1960's along the lines of work by Tilley,[21] Saint-James and de Gennes,[22] Tinkham,[23] and Yamafuji et al..[24] Tilley introduced an effective mass tensor into the linearized GL equation to account for the $H_{c2}(\theta)$ due to the conductivity anisotropy of the system. This model has been applied very successfully in systems like the Chevrel phase materials and other layered compounds which have an intrinsic conductivity anisotropy. The $H_{c2}(\theta)$ generated by this expression:

$$H,(e) = H_{c2}(\perp)/(\cos^2\theta + \epsilon^2 \sin^2\theta)^{1/2} \quad (1)$$

has a round-shaped peak with a zero derivative at the peak, as shown by the dashed-dot curve in Fig. 2. The parameter ϵ is defined with $\epsilon^2 = \sigma(\perp)/\sigma(\parallel)$, representing the conductivity anisotropy.

A second mechanism which can produce an anisotropic H_{c2} is the surface superconductivity (H_{c3}). When a magnetic field is applied parallel to the surface of a semi-infinite bulk sample the critical field $H_{c2}(\parallel)$ is enhanced over its bulk value $H_{c2}(\perp)$ by a factor of about 1.695.[22] The full angular dependence of this enhancement were approximated using a thin film (thin compared to $\xi_{GL}(T)$) geometry by Tinkham[23] by the relation:

$$|H_{c2}(\theta)\sin\theta/H_{c2}(\perp)| + |H_{c2}(\theta)\cos\theta/H_{c2}(\parallel)|^2 = 1 \quad (2)$$

where θ is measured with respect to the surface of the specimen. Later Yamafuji et al.[24] removed the thin film restriction from Tinkham's derivation and obtained a more general

relation for $H_{c2}(\theta)$:

$$|H_{c2}(\theta)\cos\theta/H_{c2}(\parallel)|^2 \cdot [1 + \tan\theta(1-\sin\theta)] + |H_{c2}(\theta)\sin\theta/H_{c2}(\perp)| = 1 \quad (3)$$

The important feature of both Eqs. (2) and (3) is that, unlike that of Eq. (1), they all produce a cusp-like peak for field parallel to the surface, as shown in Fig. 2. It should be noted that although Eq. (2) and (3) were initially derived to describe the angular dependence of H_{c3} enhancement, finite size effects in real samples can produce values of $H_{c2}(\parallel)/H_{c2}(\perp)$ larger than 1.695. In addition, H_{c3} can also be strongly suppressed by the proximity effect due, for example, to non-ideal conditions at the surface of the specimen.

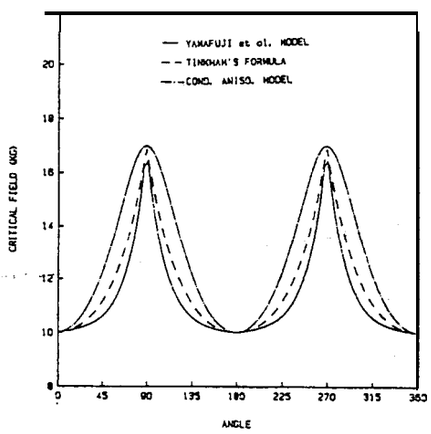

FIG. 2. The angular dependence of the upper critical field. Curves are generated using Eqs. (1)–(3) with a fixed anisotropy ratio $\epsilon = 1.695$.

In addition to the intrinsic mechanisms described above, both geometric and structural factors can also give enhancement of H_{c2} for a given field orientation. A recent paper by Dodds et al.[25] summarizes both the angular and the temperature dependencies of H_{c2} for a number of simple models that can lead to such an anisotropy as reproduced in Table I. As

TABLE I. Models fur anisotropic critical field near T_c, neglecting the paramagnetic effects. (2D and 3D denote two- and three- dimensional, respectively. The letters *i* and *a* stand for isotropic and anisotropic, respectively.) (after Ref. 25).

Model	$H_{c2}(\theta)$	$H_{c2}(T,\perp)$	$H_{c2}(T,\parallel)$	$H_{c2}^{\perp}/H_{c2}^{\parallel}$
2D(*i*)	cusp	linear	parabolic	≈ d/UT)
cylinder	bump	parabolic	parabolic	1.414
3D(*i*)	H_{c3}	linear	linear	0.59
3D(*a*)	$H_{c2}(\theta)$+H_{c3}	linear	linear	$0.59H_{c2}(\theta)$

will be seen in the following discussion, the combination of both anisotropic conductivity and H_{c3} effects (fourth row in the Table) must be solved numerically from the GL equations instead of simple multiplication as implied in the Table. In any case, it is clear that the detailed angular dependence of H_{c2} along with its temperature dependence can be used, at least qualitatively, to account for the origins of the observed H_{c2} anisotropy.

Figure 3 shows the typical H„(T) and $H_{c2}(\theta)$ data for non-columnar NbN films. As is evident from Fig.. 3(a), the linear temperature dependence in both parallel and perpendicular field orientations excludes the possibility of geometric effects as expected in Table I. Nonetheless, the angular dependencies as shown in Fig. 3(b) suggest that more

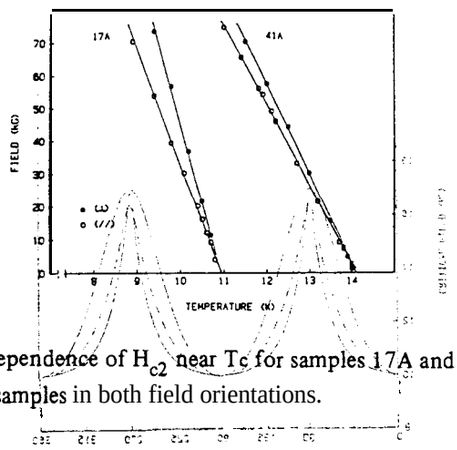

FIG. 3(a). The temperature dependence of H_{c2} near Tc for samples 17A and 41A, showing the linear behavior for both samples in both field orientations.

than one mechanisms are operative in this problem. The curve shape around the perpendicular field orientation has the clear resemblance to that produced by Eq. (1), whereas around the parallel direction a cusp-like feature is evident. Indeed, a trial fit using Eq. (1) with an appropriate anisotropy ratio ϵ accounts for the perpendicular part of the data very well (dashed curves in Fig. 3(b)). Thus, it is clear that there is a conductivity anisotropy present in these films. The cusp together with the linear temperature dependence in parallel direction suggests by itself a H_{c3} effect might be responsible. To test if this idea is indeed correct, we have made NbN films sandwiched by Aℓ-overlayers. It is well established that the H_{c3} will be significantly suppressed if the order parameter is allowed to leak into the normal regions by the proximity effect. Fig. 4 shows the $H_{c2}(\theta)$ measured for one of the normal metal sandwiched NbN films. As can be seen in Fig. 4, the cusp around the parallel field direction is removed while the overall anisotropic nature remains unchanged and can be fit by Eq. (1) satisfactorily (solid curve in Fig. 4). Since the Aℓ overlayer is quite inert to NbN (T_c of the films remains around 14 K), the effect of its presence on the formation and grain structure is expected to be minimal. The results shown in Fig. 4 thus reinforce our argument concerning the origin of the H_{c2} anisotropy in previous paragraphs. That is the overall angular dependence of the H_{c2} is a combination of the conductivity anisotropy and the H_{c3} effect.

The next question to be asked is whether the conductivity anisotropy is intrinsic to the

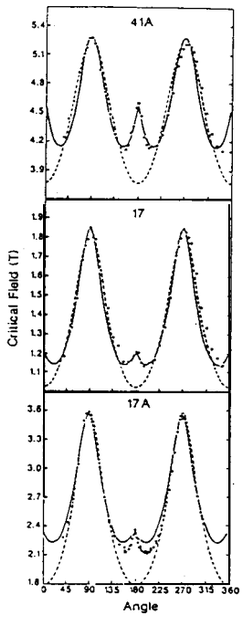

FIG. 3(b). The angular dependence of H_{c2} for three non-columnar samples. Dashed curves are fits using Eq. (1) with appropriate ϵ. Measurement temperature for each sample is: 41 A(12.5 K); 17 (12.2 K); 17A(10.3 K).

material or is due to other extrinsic effects.? To answer this question investigations on the single crystal films are necessary. Fig. 5. shows the $H_{c2}(\theta)$ results measured on a single crystal NbN films. In contrast to the polycrystalline films, the result displays a nearly ideal surface superconductivity. The solid curve is the fit using Eq.(3) with an anisotropic ratio

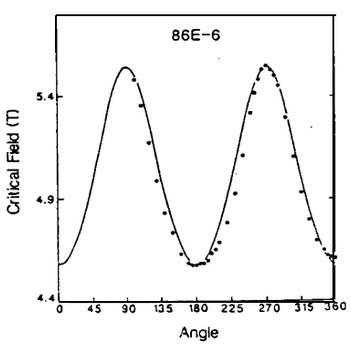

FIG. 4. The angular dependence of H_{c2} for sample made with Aℓ overlayers to suppress the H_{c3} effect. Solid curve is the fit using Eq. (1). The measurement temperature is 11 .O K with T_c = 13.6.

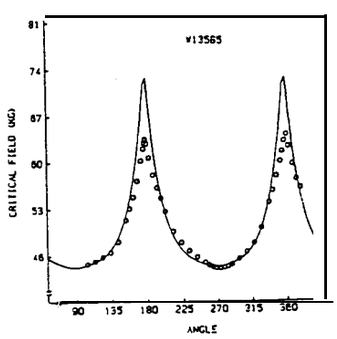

FIG. 5 The angular dependence of H_{c2} for a single crystal film shows only the H_{c3} effect. Solid curve is the fit using Eq.(3) with an anisotropic ratio of 1.7. The measurement temperature is 13.0 K with $T_c \approx 17$ K.

of 1.7. While the data near the peak position fell below the ideal H_{c3} (6) value, this slightly difference could easily be interpreted by the presence of a small degraded, or proximity, iayer on the surface of the film. In fact, the numerical fit to these data by Chin and Orlando,[26] using a non-zero order parameter gradient to reflect a non-ideal interface has shown a much better fit. The significant implication of these results is, however, obvious. It is indicative that the conductivity anisotropy needed to account for the $H_{c2}(\theta)$ of the polycrystalline films is not intrinsic to the material. The conductivity anisotropy must be originated from the specific microstructure of the films, which also explains the sample dependence of the ratio ϵ (cf. Fig. 3(b)). To further elucidate this point, Fig. 6. shows the $H_{c2}(\theta)$ data for a film of known microstructure[27] with the grains being inclined to the

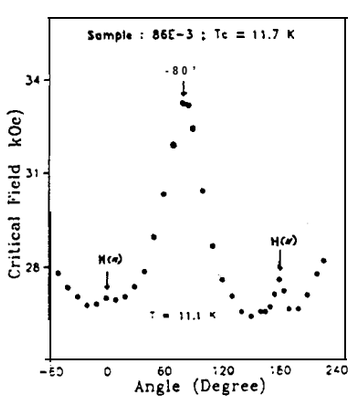

FIG. 6. The angular dependence of H_{c2} for sample 86E-3 (T_c = 11.7 K) with a inclined grain structure. The result demonstrates the effect of the grain morphology on $H_{c2}(\theta)$.

normal of the substrate surface. As can be seen the peak position of the perpendicular orientation shifts from the normal direction by about 10°, whereas the position of the cusp-peaks remains exactly parallel to the film surface. The asymmetrical appearances in the peak heights are believed to be of the same origin.

To complete the analysis of the overall $H_{c2}(\theta)$ for the polycrystalline films it seemed necessary to develop a model which combines both an overall anisotropy in conductivities with the H_{c3} effects. While this problem can only be solved numerically, an analytical solution which reproduces all the qualitative features of the full three dimensional solution has been worked out.[28] Briefly, the anisotropic effective mass tensor is built in the derivation of the $H_{c3}(\theta)$ within the framework of the GL equations. The resulting formula has the same form as that derived by Tinkham[23] (Eq. (2)), except that the anisotropic nature is adhered in the derivation. Consequently, the anisotropic ratio ϵ used must be explicitly determined from the experiment. The solid curves displayed in Fig. 3(b) are generated by this equation with the measured values of H_{c2} (II) and H_{c2} (I) as the only input parameters. As can be seen clearly, it reproduces both the general features and the magnitude of the $H_{c2}(\theta)$ very well. It must be emphasized, however, that the full account of the overall $H_{c2}(\theta)$ should always rely on the detailed numerical calculation of the GL equations. In

any case, the results thus far presented strongly suggest that the detailed microstructure of the films plays an important role in the H_{c2} anisotropy of this material. Although we do not have the direct evidence for what causes the conductivity anisotropy assumed to account for the data, it is expected to be due to the same origin: the microstructure effects. As a major consequence, the grain boundary resistance must be involved in determining the supposedly "intrinsic" superconducting property, H_{c2}, at least in the temperature range studied.

II-3 Summary: The H_{c2} Anisotropy of The NbN Thin Films

In the first part of this report, we have resolved the outstanding problem of the H_{c2} anisotropy commonly observed in reactively sputtered NbN thin films. The ***ad hoc*** theory based on the geometric enhancement effects proposed by Ashkin and co-workers was proved to be inadequate. We conclude that to understand the mechanisms responsible for the critical field anisotropy of a cubic structured thin film superconductor, the film microstructure, the temperature dependence of the H_{c2} (near T_c), and the explicit angular dependence of the H_{c2} must be all considered. It is believed that the overall conductivity (including the grain boundary resistivity) in the normal state is involved in determining the critical field of the superconductor. More importantly, it is clearly demonstrated that, regardless the detailed microscopic mechanism, the GL phenomenological theory is useful in accounting for the physical parameters of the superconductivity. It is this conclusion that has motivated us to apply the same concept to the study of the high-T, oxide superconductors.

III. OXIDE SUPERCONDUCTORS

In this part of the report we will present some of the preliminary studies on the H_{c2} anisotropy of the newly discovered high-T, oxide superconductors. The main idea is to extend the concept developed in the previous part and apply it to these new superconductors. It is hoped that some meaningful results can be extracted by this way, while the microscopic mechanisms for high-T, superconductivity is still indecisive.

III-1 The Effects of Al Substitution in The H_{c2} of YBCO Single Crystals

Single crystal $YBa_2Cu_3O_{7-\delta}$ and $YBa_2Cu_{3-x}Al_xO_{7-\delta}$ were used to study the H_{c2} anisotropy of these materials. Crystals of BYCO and its derivatives were prepared by Dr. L. F. Schneemeyer[29] of Bell Laboratories using a partial melting technique (CuO rich), then post-annealed for a long period of time ($\approx$ 600 hrs) in flowing oxygen to maximize the oxygenation. Al is introduced as a constituent of the melt (e.g. as $Al(NO_3)_3$) contained in a less reactive crucible, such as zirconia crucible. Single-crystal x-ray diffraction studies[30] have established that Al substitutes on the Cu-0 chain site in $YBa_2Cu_3O_7$, and along with thermogravimetric analysis that AQ-substitution does not significantly increase the oxygen stoichiometry, at least up to an Al fraction $x = 0.4$ in $YBa_2Cu_{3-x}Al_xO_7$. For $x \leqslant 0.1$ the

full-oxygenated pseudoquaternary has orthorhombic symmetry ($a_o \neq b_o$), while for x > 0.1 the material becomes tetragonal and the T_c of the crystal decreases much more rapidly than when $x \leq 0.1$. It seemed that in order to gain insight into the maximum effect of Aℓ on the H_{c2} anisotropy without the complication of accompanying structure transition, single crystals with x = 0.1 would be the best choice. Consequently, only the results of undoped $YBa_2Cu_3O_7$ and $YBa_2Cu_{2.9}Aℓ_{0.1}O_7$ will be presented.

The room temperature resistivity in $YBa_2Cu_{2.9}Aℓ_{0.1}O_7$, ρ_{ab} (300 K) ≈ 500 μΩ-cm, is identical to the resistivity typically found in undoped $YBa_2Cu_3O_7$ crystals,[31] and is comparable to values quoted in other work.[32] However, the resistivity is not linear in temperature.[31] As a result, the resistivity just above T_c, $\rho_{ab}(T_c) \approx 100$ μΩ-cm, for the doped samples is less than that of the undoped crystal ($\rho_{ab} \approx 160$ μΩ-cm). The superconducting transition is about 2 K wide (10%–90%) for the doped crystals, which is broader than that obtained in undoped crystals (typically 0.3 K wide, centered at 88.5 K). When a magnetic field in the range 1 O-l 00 kOe is applied parallel to the c-axis, the transitions are found to broaden as commonly observed, but surprisingly, the broadening is substantially less than obtained in undoped crystals.[31] There have been two different mechanisms proposed to explain the transition broadening in field: giant flux creep due to the small pinning energy[33] and the critical fluctuations.[34] Both theories, though very different in physics, are based on the short coherence length in this material. As will be seen in the following, from the measurements of the $H_{c2}(T)$ and $H_{c2}(\theta)$, doping Aℓ will increase the a-b plane coherence length ξ_{ab} by as much as 2.5 times, which seems to be consistent with the observations described above. That is doping Aℓ can either enhance pinning of the flux line or suppress the critical fluctuation by increasing the coherence volume, $\xi_{ab}^2 \cdot \xi_c$, which in turn sharpen the resistivity transitions in field.

Doping by Aℓ has a dramatic effect on the upper critical field, as shown in Figs. 7. and 8. We defined H_{c2} as the field required to return the resistance to half of its extrapolated

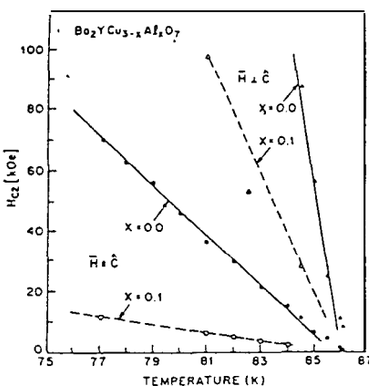

FIG. 7. The temperature dependence of H_{c2} for $YBa_2Cu_3O_7$ and $YBa_2Cu_{2.9}Aℓ_{0.1}O_7$ single crystals. The solid lines represent the linear fits for the undoped sample, whereas the dashed lines are fits for the AP-doped sample. Data taken at fields up to 200 kOe (not shown) were used to obtain the indicated linear fits.

normal-state value, as commonly used in the conventional superconductors. Fig. 7. shows the temperature dependence of H_{c2} for both undoped and U-doped crystals with field applied parallel and perpendicular to the c-axis of the crystal. Clearly, the H_{c2} of the Aℓ-doped sample is significantly reduced, especially for H‖c. Except for very close to T_c where positive curvature possibly due to inhomogeneity or fluctuation effects is observed, the $H_{c2}(T)$ can be reasonably fitted by a straight line (solid lines in Fig. 7). We infer the zero

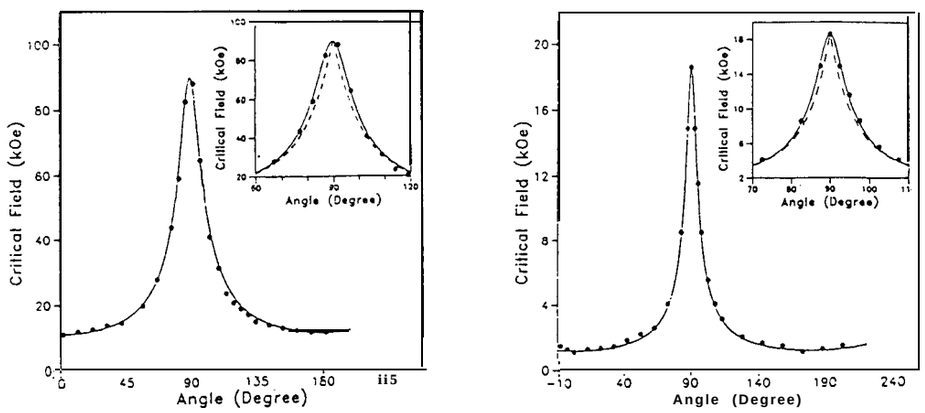

FIG. 8. The angular dependence of H_{c2} for both the (a) undoped and (b) Aℓ-doped YBCO single crystals. The solid curves are fits using Eq. (1) with $\epsilon = 8.0$ and ϵ 15.5 for the undoped and AP-doped crystals, respectively. The insets compare the fits with Eq. (1) and Eq. (2) for both cases.

temperature coherence length $\xi(0)$ from these slopes by first calculating the orbital critical field H^{*}_{c2} (0) for each field direction, using the WHH-Maki[35] theory: $H^{\perp,\parallel}_{c2}(0) = 0.693\, T_c[(dH^{\perp,\parallel}_{c2}/dT)|_{T_c}]$. The coherence lengths are then obtained by using: $\xi^2_{ab}(0) = \phi_0/2\pi H^{\parallel}_{c2}(0)$ and $\xi_c(0) = \phi_0 H^{\parallel}_{c2}(0)/2\pi[H^{\perp}_{c2}(0)]^2$, with $\phi_0 = 2.07 \times 10^{-7}$ gauss-cm^2 bemg the flux quantum. The results are summarized in Table II, together with some other physical properties of these crystals. As is evident from these rough estimates, ξ_c is essentially unchanged by All-doping, whereas a dramatic and unequivocal increase in ξ_{ab} is observed (see Table II).

TABLE II. Parameters inferred for YBa_2Cu_3 0, and $YBa_2Cu_{2.9}A\ell_{0.1}$ 0, single crystals. H_{c2}' is the critical field slope near Tc.

	T_c	$\rho_{ab}(T_c)$	$H'_{c2\parallel}$	$H'_{c2\perp}$	$\xi_{ab}(0)$	$\xi_c(0)$	anisotropy
	K	μΩ-cm	kOe/K	kOe/K	n m	nm	–
Ba_2YCu_3 0,	88.5	160	7.0	54	2.8	0.36	7.8
$Ba_2YCu_{2.9}A\ell_{01}O_7$	84	100	1.3	20	6.5	0.42	15.5

Figure 8(a) shows the $H_{c2}(\theta)$ for the undoped YBa_2Cu_3 0, single crystal measured at 84.5 K (T, of this sample is 88.5 K). It is noted that the sensitivity of H_{c2} value to the field orientation was also utilized to precisely determine the H∥c and H⊥c orientations, as shown in Fig. 7. Clearly, the data can be described very well by the conventional three-dimensional effective mass model (Eq. (I), solid curves in the figure), indicating the intrinsic conductivity anisotropy in this material. The inset in Fig. 8(a) expands the scale around the H⊥c orientation. The dashed curve in the inset is a fit by Eq. (2) with the same anisotropy ratio, $\epsilon = 8$. As can be seen the fit is not as good as the solid curve suggesting that the property is three-dimensional, at least in the temperature range measured. Fig. 8(b) shows the $H_{c2}(\theta)$ for the $YBa_2Cu_{2\,9}A\ell_{0\,1}$ 0, crystal measured at 80.5 K (the T_c of this sample is 84 K). Again the data were fit very well by Eq. (1) and the inset compares the fits for two different models mentioned above. Despite almost a factor of 2 increase in teh anisotropy ratio ($\epsilon = 15.5$ in this case), there is no evidence of two-dimensional-like behavior. This is consistent with the fact that, although the crystal has been driven toward tetragonal, the lattice constant along the c-axis (hence the distance between the Cu-0 planes) has not been affected by Aℓ-doping.[36] Thus the increase in the H_{c2} anisotropy is again attributed to the dramatic increase in ξ_{ab} and not to a "thin-film" geometric enhancement.

To further explore the possible origins of the unusual change in ξ_{ab} by M-doping, we consider the full GLAG relationship for ξ_{GL} (0) in terms of microscopic parameters[37]:

$$\xi_{ab}(0) = [2.9 \times 10^{32} T_c^2 \gamma^2 (n^{2/3} S/S_F)^{-2} + 1.6 \times 1\,0^{12} \rho_{ab} \gamma T_c]^{-1/2} [R(\Gamma_{tr})]^{1/2} \text{ cm} \quad (4)$$

$$P_{ab} = 1.27 \text{ X } 10^4 [\ell_{tr} (n^{2/3} \text{ S/S,})]^{-1} \quad \Omega\text{-cm} \quad (5)$$

Where n is the conduction electron density (cm^{-3}), S_F is the Fermi surface area of a free electron gas of density n, S is the real Fermi surface, γ is the normal state electronic specific heat coefficient, $\Gamma_{tr} \equiv \hbar w_F / 2\pi k_B T_c \ell_{tr}$ (where ℓ_{tr} is the electron mean free path), $R(\Gamma_{tr})$ is related to the Gor'kov x-function and is bounded between 1.O and 1.17 in the dirty and clean limits, respectively, and other symbols have their usual meanings. The first term in Eq. (5) reflects the BCS coherence length (i.e. in the clean limit), whereas the second term introduces the effect of transport scattering and dominates in the dirty limit ($\Gamma_{tr} >> 1$). The increase in ξ_{ab} is qualitatively consistent with the decrease in ρ_{ab}(Tc), which is ≈ 100 μΩ-cm for the doped crystal and ≈ 160 μΩ-cm for the undoped samples. However, leaving aside the issue of how increasing the crystal disorder (by doping Aℓ) could decrease rather than increase ρ_{ab}, *we* note ρ_{ab} decreases only by a factor of 1.6, which would increase ξ_{ab} by a factor of at most $(1.6)^{1/2} \approx 1.3$ in the extremely dirty case. Since this is far less than the observed two-fold increase, we infer that other parameters such as γ, T_c, and/or $n^{2/3}$ S/S, must be significantly altered by AP-doping. As the T_c and hence γ is only affected slightly, which leads to the conclusion that $n^{2/3}$ S/S, must increase by a factor of 1.6–2.0.[31] Such a change would presumably be driven by disorder on the Cu-0 chain sublattice, the introduction of new Aℓ-O bonding states, and perhaps the change in the symmetry of the crystal. Indeed, it has been shown,[38] from the tight-binding band structured claculation,

that for a complete substitution of Al on Cu(1) site the change in band structure is dramatic. Unfortunately, theoretical calculations on partial substitution with AR are not available at present, thus direct comparison with this observation remains inconclusive. Nonetheless, so large a change in S is surprising, since with such a change it is hard to imaging why ξ_c and T_c were affected so little. Further studies are certainly needed to further reconcile this remarkable behavior.

III-2 **Anisotropic Current-Voltage Characteristics in Single Crystal** BSCCO

The non-rare-earth-based compound Bi, $Sr_2Ca_1Cu_2O_{8+\delta}$ (BSCCO) has provided another member of the cuprate family to study. The single crystals we used were grown from alkali chloride fluxes by Dr. L. F. Schneemeyer. Details of the preparation procedures can be found elsewhere.[29] Structurally, this compound differs from the YBCO superconductors in several respects. The Cu-0 chains found in YBCO are replaced by Bi-0 edge-shared tetrahedra in BSCCO, perhaps leading to more two-dimensional-like behavior in the latter system. In a sense it should have a similar effect to All-doping in YBCO in terms of removing the contribution to the superconductivity from the Cu-0 chains. The pair of Cu-0 planes believed to be central to the superconductivity in these materials are apparently more weakly coupled than in undoped YBCO, as suggested by the larger anisotropy in the conductivity. This is expected to be even more dramatic in BSCCO due to the much larger lattice spacing along the c-axis of this material. Finally, unlike YBCO, there is no twinning in the a-b plane in this system. It is therefore interesting to see how these structural parameters affect the superconducting properties as compared to YBCO system.

Although, qualitatively we expect BSCCO to have characteristics similar to those of YBCO, the "critical field" results found in this material are not easily interpreted in terms of conventional definitions. In an earlier publication[39] we have reported some of the results on the angular dependence of the magnetic-field-induced resistive transition in single crystal BSCCO with T,(O) typically of 84 K. The peculiar characteristics of those resistive transitions and the inability of using Eq. (1)-(3) to account for the angular dependence of the "critical field" were attributed to the immediate flux motion even in vanishingly small applied current and magnetic field. The virtually non-existing pinning in this material has been the subject of extensive investigations. The Kosterlitz-Thouless vortex-unbinding transition[13] and flux-lattice-melting[14] at temperatures far below T_c are among the possibilities proposed recently.

Figure 9. shows a typical example of the immediate flux motion effect measured at 77 K with an applied field of 1 kOe as a function of the angle between the field direction and the c-axis of the crystal. As can be seen in the figure, even at a temperature far from T_c a nearly straight I-V characteristic in the low current regime is evident for angles smaller than 60°, indicating a Bardeen-Stephen-like flux-flow behavior existing in this material. According to the Bardeen-Stephen model the flux-flow resistivity (i.e., the slope of the I-V curve) can be a direct measure of the H_{c2} at the measuring temperature. Indeed, a consentient determination of the $H_{c2}(T)$ made from this kind of measurement and other methods can be obtained, at least in the H‖c orientation where the slope can be determined relatively

unambiguously.[40] It is also interesting to note that the anisotropy ratio in the critical current density (defined by an 1 μV/cm criterion) between H$\|$c and H$\perp$c is larger than 100. A value much larger than those reported for other oxide superconductors and is consistent with our expectation from the more two-dimensional crystal structure for this material.

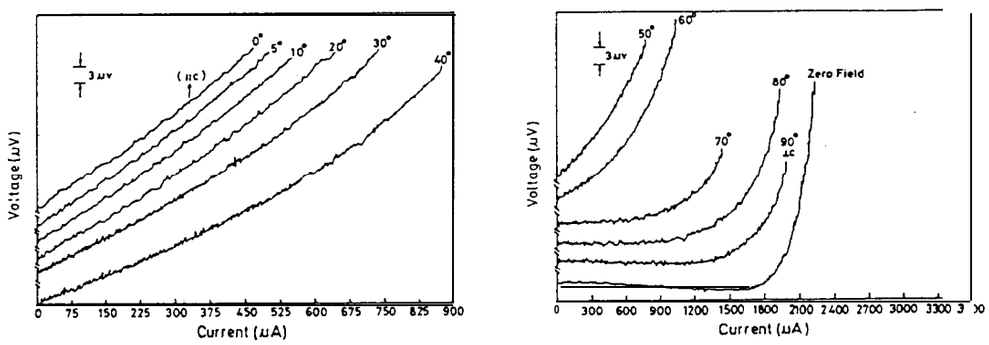

FIG. 9. The angular dependence of the I-V characteristics for single crystal $Bi_2Sr_2Ca_1Cu_2O_{8+\delta}$ measured at liquid nitrogen temperature with an applied field of 1 kOe. Also shown is the zero field I-V with the current flowing in the ab-plane in all cases.

IV. SUMMARY

In this report we have demonstrated how the superconducting properties can be affected by both the microstructures and crystal structures of the materials with detailed analyses of the upper critical field anisotropies using the Ginzburg-Landau phenomenological theory. It is shown that the critical field anisotropy and its angular dependence for the sputtered NbN thin films are due to the combining effects of conductivity anisotropy originated from the grain boundary resistivity and the surface superconductivity. For the oxide superconductors, especially the YBCO crystals, the anisotropy is due to the intrinsic nature of the layered crystal structure. The effect of Al-doping in YBCO suggests a dramatic change in the band structure and further investigations in this subject may eventually lead to rich insight into the origin of the high-T, superconductivity. The BSCCO system, on the other hand, displays its own nature and can be an excellent system for studying the fundamental properties of flux flow and its effects on superconducting properties.

ACKNOWLEDGEMENTS

The author would like to express his appreciations to Prof. D. A. Rudman, Prof. T. P. Orlando, Dr. R. B. van Dover. Dr. L. F. Schneemeyer, Dr. J. Talvacchio, and Dr. D. W. Capone II for their stimulating discussion and generous support of the samples. The hospitality of the National Magnet Laboratory during the course of this work is also gratefully acknowledged.

REFERENCES

1. R. T. Kampwirth, D. W. Capone II, K. E. Gray, and A. Vincens, IEEE Trans. Magn. MAG-21,459 (1985).
2. M. Dietrich, IEEE Trans. Magn. MAG-21, 455 (1985).
3. S. Kasaka, A. Shoji, M. Aoyagi, S. Shinoki, S. Tahara, H. Ohigashi, H. Nakagawa, S. Takada, and H. Hayakawa, IEEE Trans. Magn. MAG-21, 102 (1985).
4. J. C. Villegier, L. Vieux-Rochaz, M. Goniche, P. Renard, and M. Vabre, IEEE Trans. Magn. MAG-21,498 (1985).
5. H. Hayakawa, Phys. Today 39, 46 (1986).
6. J. W. Ekin, J. R. Gavaler, and J. Greggi, Appl. Phys. Letts. 41, 996 (1982).
7. P. Gregshammer, H. W. Weber, R. T. Kampwirth, and K. E. Gray, J. Appl. Phys. 64, 1301 (1988).
8. J. Y. Juang, D. A. Rudman, J. Talvacchio, and R. B. van Dover, Phys. Rev. B38;2354 (1988).
9. J. R. Gavaler, J. Talvacchio, and A. I. Braginski, "Advances in Cryogenic Engineering", Vol. 32, Plenum, N.Y., 659 (1986).
10. B. Oh, K. Char, A. D. Kent, M. Naito, M. R. Beasley, T. H. Geballe, R. H. Hammond, A. Kapitulnik, and J. M. Graybeal, Phys. Rev. B37, 7861 (1988).
11. Y. Yeshurun and A. P. Malozemoff, Phys. Rev. Letts. 60, 2202 (1988).
12. N. C. Yeh and C. C. Tsuei, Phys. Rev. B39, 9708 (1989).
13. S. Martin, A. T. Fiory, R. M. Fleming, G. P. Espinosa, and A. S. Cooper, Phys. Rev. Letts. 62, 677 (1989).
14. P. L. Gammel, L. F. Schneemeyer, J. V. Waszczak, and D. J. Bishop, Phys. Rev. Letts. 61, 1666 (1988).
15. D. D. Bacon, A. T. English, S. Nakahara, F. G. Peters, H. Schreiber, W. R. Sinclair, and R. B. van Dover, J. Appl. Phys. 54, 6509 (1983).
16. H. L. Ho, R. T. Kampwirth, K. E. Gray, D. W. Capone II, and L. S. Chumbley, Ultramicroscopy 22, 297 (1987).
17. J. Talvacchio and A. I. Braginski, IEEE trans, Magn. MAG-23, 859 (1987).
18. D. A. Rudman, J. Y. Juang, R. B. van Dover, S. Nakahara, D. W. Capone II, and J. Talvacchio, IEEE Trans. Magn. MAG-23, 83 1 (1987).
19. R. R. Hake, Appl. Phys. Letts. 10, 189 (1967).
20. M. Ashkin, J. R. Gavaler, J. Greggi, and M. J. Decroux, J. Appl. Phys. 55, 1044 (1984).
21. D. R. Tilley, Proc. Phys. Soc. (London) 85, 1177 (1965); 86, 289 (1965); 86, 678 (1965).
22. D. Saint-James and P. G. de Gennes, Phys. Letts. 7, 306 (1963).
23. M. Tinkham, Phys. Letts. 9. 217 (1964).
24. K. Yamafuji and F. Irie. Phys. Letts. A25, 387 (1967); K. Yamafuji, E. Kusayanagi, and F. Irie, Phys. Letts. 21, 11 (1966).
25. S. A. Dodds, S. N. Harrington, R. S. Newrock, and K. Loeffler. Phys. Rev. B33, 3 115 (1986).

26. C. C. Chin and T. P. Orlando, Phys. Rev. B37, 5811 (1988).
27. J. Y. Juang, K. Barmak, D, A. Rudman, and R. B. van Dover, J. Appl. Phys. 66, 3 136 (1989).
28. J. Y. Juang, Ph. D. Thesis, Massachusetts Institute of Technology, 1989, Chap. 4. (unpublished).
29. L. F. Schneemeyer et al., Nature 332, 442 (1988).
30. S. A. Sunshine et al., Phys. Rev. B38, 893 (1988).
31. R. B. van Dover, L. F. Schneemeyer, J. V. Waszczak, D. A. Rudman, J. Y. Juang, and J. A. Cutro, Phys. Rev. B39, 2932 (1989).
32. Y. Iye, T. Tamegai, H. Takeya, and H. Takei, Physica 148B, 224 (1987).
33. M. Tinkham, Phys. Rev. Letts. 61, 1658 (1988).
34. K. Kitazawa, S. Kambe, and N. Okazaki, "Progress in High Temperature Superconductivity" Vol. 19, edited by P. T. Wu et al., World Scientific, Singapore, 1989. P. 79.
35. N. R. Werthamer, E. Helfand, and P. C. Hohenberg, Phys. Rev. 147, 295 (1966); K. Maki, Phys. Rev. 148, 362 (1966).
36. J. M. Tarascon et al., Phys. Rev. B37, 7459 (1988).
37. T. P. Orlando, E. J. McNiff Jr., S. Foner, and M. R. Beasley, Phys. Rev. B19, 4545 (1979).
38. B. A. Richer-t and R. E. Allen, Phys. Rev. B37, 7496 (1988).
39. J. Y. Juang, J. A. Cutro, D. A. Rudman, R. B. van Dover, L. F. Schneemeyer, and J. V. Waszczak, Phys. Rev. B38, 7045 (1988).
40. J. Y. Juang, J. A. Cutro, and D. A. Rudman, (unpublished).